Artificial soft cilia with asymmetric beating patterns for biomimetic low Reynolds number fluid propulsion

Edoardo Milana[+], Benjamin Gorissen[+], Sam Peerlinck, Michael De Volder* and Dominiek Reynaerts

E. Milana, Dr. B. Gorissen, S. Peerlinck, Prof. M. De Volder, Prof. D. Reynaerts
Department of Mechanical Engineering, KU Leuven and Flanders Make, Celestijnenlaan 300, 3001 Leuven, Belgium
Prof. M. De Volder Institute for Manufacturing, Department of Engineering, University of Cambridge, 17 Charles Babbage Road, Cambridge CB3 0FS, UK
[+] Equal contributions
* E-mail: mfld2@cam.ac.uk

Nature's evolutionary mechanism devised an elegant solution to liquid propulsion in low Reynolds regimes: arrays of beating cilia. Various motion asymmetries evolved in these hair-like organelles to achieve Stokes flow. In particular, spatial asymmetry, where a different trajectory occurs in the cilium's effective and recovery stroke, is an efficient way of generating low Reynolds fluid flow. However, this type of asymmetry is difficult to mimic and control artificially, especially when it concerns the in-plane movement of a type of biological cilia. In this paper, we propose for the first time an artificial pneumatic soft cilium that allows for adjustable spatial asymmetry. The developed cilium is fabricated using polydimethylsiloxane (PDMS) moulding and comprises two embedded soft pneumatic actuators. These inflatable actuators are independently controllable to tune the spatial asymmetry in the cilium's beating pattern. Using low Reynolds number flow measurements, we confirm that spatial asymmetry is a necessary condition for generating fluid propulsion. Further, the induced flow rate can be influenced by changing the amount of spatial asymmetry, where fluid speeds of up to 0.04 mm min^{-1} were registered in glycerol at an actuation frequency of 250 mHz. To our knowledge, this is the first report of an artificial pneumatic cilium with tuneable spatial asymmetry exhibiting an in-plane deformation, and it is an

important step forward in the mimicry of biologic viscous propulsion strategies and in the understanding of their fluid transport mechanisms.

1. Introduction

Ciliary propulsion emerged in nature as an efficient mechanism to propel fluids in low Reynolds number conditions [1]. These hair-like cells evolved independently in different organisms, leading to a multitude of applications domains, all sharing the same basic topology. As such, they can be found on the membrane of ciliates [2], inside the tracheae of mammals [3], and on the tentacles of Ctenophores [4]. Due to the small dimensions of these cilia, the interaction with the surrounding fluid is dominated by viscous forces, reducing the role of inertial effects. As a result, the equations of motion become time reversible and reciprocal motion is unable to generate a net propulsion [5]. Thus, motion asymmetries are essential to generate net flow. These asymmetries can be created at the level of a single cilium as well as for whole cilia arrays. For a single cilium, orientational, temporal and spatial asymmetry can be distinguished [6], where the latter has the highest impact on low-Reynolds fluid propulsion. Spatial asymmetry, where the cilium tip describes a different path during the effective and recovery stroke, is quantified by the swept area; the larger the area, the higher the net flow [7]. At the array level an additional type of asymmetry has been observed, metachronal asymmetry, which is characterized by a phase difference between neighboring cilia [8] that gives rise to a global wave-like movement.

With the development of microsystem technology, artificial cilia can now be fabricated and are foreseen to find applications in microrobotic devices, such as microswimmers [9,10], microsensors [11], micropumps [12–14] and micromixers [15–18]. The vast majority of artificial cilia consist of microactuators that are incorporated in silicone rubber pillars or plate-like flexible structures in order to mimic the biological hair-like design. Current actuation methods include electric fields [15], magnetic fields [19–23], vibrations [24,25], mechanical forces [26] or

pressurized fluids [27,28]. However, asymmetric motion remains the most challenging feature to mimic in artificial cilia systems. In nature, nonreciprocal beating is achieved by a change in bending stiffness between the effective and recovery stroke [29]: a higher stiffness is observed during the fast effective stroke, where the cilium does not deform significantly, whereas in the slower recovery phase the cilium has a lower stiffness and tends to be deformed by the drag forces. To mimic such an asymmetric motion, the artificial cilium needs at least two deformation modes that need to be sequentially addressed. This can be achieved through elastic instabilities [7], the interaction between elastic, viscous and actuation forces [26,30], or a multi-segmented cilium [31,32] where each segment is individually actuated. Rod-like magnetically-actuated cilia have been reported to achieve spatial asymmetry [19,20,22,33,34], by applying an external magnetic field to rotate tilted cilia, resulting in a cone shaped elastic deformation path. Further, plate-like magnetic cilia [21,35,36] showed an enhanced planar swept area, very similar to the one observed in Paramecium [2], due to the interplay between stored elastic energy and the magnetic field. However, this interplay between different forces makes it difficult to precisely tune the magnitude of the various asymmetric motions separately. Hanasoge *et al* [36] showed how the swept area varies by changing the actuation frequency or the amplitude of the magnetic field, but this variation has also an impact on the orientation angle. Moreover, the phase difference between neighboring magnetic cilia is difficult to control, due to the spatial homogeneity of magnetic fields. For this reason, researchers proposed an array of different cilia with increasing length [37] to be able to form metachronal motion. Overall, magnetic cilia are a good candidate for creating biomimetic fluidic propulsion, but they do not allow to unravel the effects of the various asymmetries, and are therefore limited in the ability of studying the mechanism behind the fluid transport. As an alternative, this work focusses on cilia driven by elastic inflatable actuators (EIAs), which have a great potential for mimicking natural cilia, since their motion upon inflation can be designed for [38]. Further, they can be miniaturized [39] and are mechanically similar to

biological cilia, consisting out of soft materials. Moreover, these actuators could be compatible in future developments in the field of soft robotics, including surgical tools [40–42], robotic grippers [43–45], high-Reynolds swimmers and walking robots [46]. Here, we propose a new pneumatic cilium design, which allows to introduce spatial asymmetry by incorporating two individually addressable EIA actuators [47,48] in each cilium. These two degrees-of-freedom (DoF) pneumatic cilia can be programmed to generate a large swept area between the forward stroke and the recovery stroke like biological cilia. Further, they are fabricated using a single step micromoulding process, which enables a precise control over its dimensions. The proposed artificial cilia are novel as they allow to control spatial and orientational asymmetry separately, which permits to measure experimentally the effect of each asymmetry on fluid flow in low-Reynolds regimes. This is tested by both tracking the overall fluid flow using ink dye tests, and 2-D Particle Image Velocimetry (PIV) to obtain a quantitative measurement of the net fluid flow. Although the size of the developed cilium is larger than biological cilia, by matching Reynolds number and deformation, the reported results are invariant to the physical scale.

2. Design and operation of soft artificial cilia

The developed artificial cilia consist of two bending actuators integrated into a single monolithic structure, each actuator is independently addressable by a dedicated pressure source. As shown in **Figure 1a**, each actuator consists of an asymmetric inflatable cavity, but the actuators differ in length, so that an inflation of the longest causes the cilium to curl up, and the inflation of the shortest tilts it forwards. By inflating both actuators with a phase difference, the tip of the cilium traces a non-zero swept area, that can be adjusted by the phase lag between the actuators. The cilium is 1 mm in diameter, and the actuators are 16 mm and 6 mm long. The long segment has an internal void of 0.6 mm in diameter and 0.14 mm eccentricity, to ensure optimal bending deformation [48]. The shorter pillar has an internal

4

cavity of 0.76 mm in diameter with an eccentricity of 0.06 mm, which results in the same bending coefficient as the long segment, referring to the definition of bending coefficient given by Gorissen [46] et al. This design is validated through a static finite element simulation using the commercial code ABAQUS, which has been also used to identify the optimal driving pressures to guarantee sufficient swept area, while not exceeding yield stresses as explained in the SI. The beating motion is simulated with a fluid-structure interaction method: the two inner cavities are initially completely filled with an incompressible fluid, and the inflations are simulated by increasing the fluid volumes inside the cavities, causing the structure to deform. This technique facilitates monitoring inner pressures and volumes [49]. A hyperelastic incompressible Neo-Hookean model (μ=0.68 MPa) has been implemented to describe the mechanical properties [50] of PDMS according to the curing conditions of the manufacturing process. The nonlinear bending radius vs. pressure relationship (**Figure S1b**), caused by the hyperelasticity of PDMS, sets limits to the pressure values that can be used. In these simulations pressures above 145 kPa for the long segment drastically increase the bending radius sensitivity to pressure, indicating that slight variations of pressure above those limit values cause sudden and incontrollable increases in deformation that can lead to failure. For these reasons, we determined as maximum actuating pressures 100 kPa for the short segment (p_S) and 140 kPa for the long one (p_L). As shown in **Figure 1b** the cilium is driven by two linear pressure ramps with maximum pressure values p_S and p_L. The period of both the pressure waves is identical, however in order to optimize the cilium's swept area, we have studied the impact of a phase difference between the two pressure waves on the outlined tip motion. Using finite elements analysis, the actuator is loaded several times for different phase shifts of the pressure profiles. The results of this analysis, as depicted on **Figure 2a-2b**, show an increase in swept area with phase shift, from zero when the two waves are synchronous (symmetric motion) up to a maximum when the phase shift is equal to 90°, while the

orientation angle does not vary. In this way it is possible to tune the spatial asymmetry without changing the orientational asymmetry.

Experimentally, this optimal actuation scheme is imposed by inflating the long segment to a max pressure, p_L, of 140 kPa and the short segment with a max pressure, p_S, of 100 kPa with a 90° phase difference. The cilium shows a deformation resembling that of a natural cilium, as illustrated in **Figure 2c**. By superimposing the four images and connecting the positions of the tip, the swept area between the green line (inflation) and the red line (deflation) can be measured (**Figure 2d**). In contrast, a simultaneous increase of p_s and decrease of p_L or vice versa leads to a reduced swept area, as are shown on respectively **Figure 2e** and **Figure 2f**. The decrease in swept area in the latter case is caused by the contribution to a negative stroke at the end of the inflation of the long actuator, which suddenly bends due to the incontrollable overpressurization predicted by the FEM simulations.

3. Propulsion measurements

To measure the net flow achieved by the cilium, they are mounted in a D-shaped closed-loop channel, filled with glycerol (see Materials and Methods). An ink dye is introduced in the flow channel and traced over time as different actuation patterns are imposed to the cilium, to differentiate between spatial symmetric and asymmetric motion. At a beating frequency of 125 mHz, the Reynolds number is approximately 0.02 (see calculations in SI), which matches that of microorganisms [51] and the Stokes flow condition. The results of the dye tracing tests are summarized on **Figure 3**, where the deformation of cilia is displayed, showing respectively no spatial asymmetry and spatial asymmetry. At the beginning of the tests, ink lines were injected in the channel, which are displayed in yellow in the figure. Using an image editing software, these ink lines have been superimposed on top of the images taken after *n* consecutive cycles (125 mHz), where n= 150 for the symmetric case (**Figure 3a**) and n=130 (**Figure 3b**) for the asymmetric case. For symmetric actuation, there is no significant motion

of the ink lines visible, which proves that the fluid is moving equally back and forward during the effective and recovery stroke, as is expected for a symmetric actuation pattern in laminar conditions [5]. When the cilium beats asymmetrically, on the other hand, it is possible to observe a net fluid flow along the direction of the beating cilium (i.e. to the right in **Figure 3b**). Note that in order to stay in a laminar regime, the beating frequency is slow, and therefore the actuation tests last about 20 min, during which the ink lines diffuse slightly. This effect was enlarged by the leakage of actuation fluid (air) through the cilium wall, distorting the ink lines close to the cilium.

Although the symmetrically driven cilium does not exhibit spatial asymmetry, it does show orientational asymmetry, as its mean deformation is tilted away from the surface normal. Therefore, these tests conclude that orientational asymmetry is not sufficient to create a net flow propulsion at low Reynolds numbers. These results corroborate the theoretical results by Khaderi [6] et al., who showed that spatial, orientational and temporal asymmetry all have an impact for flows with Re > 1, whereas the role of orientational and temporal asymmetries progressively reduces and is disappearing for Re < 0.1 (Stokes flow), making spatial asymmetry indispensable for fluid propulsion, in accordance with the Scallop theorem [51]. This research shows an experimental validation of Khaderi's work, capturing net fluid flows in the same plane as the cilium movement occurs.

4. Flow field measurements

This section reports 2D PIV tests that were conducted to study the influence of different types of asymmetry on the flow field. Previous work on artificial cilia almost exclusively report PIV measurements in a 2D plane orthogonal to the cilia implantation direction [21,34,52]. Khaderi et al. [6] showed via theoretical modeling that the mechanism of fluid propulsion can be explained by visualizing the flow surrounding the cilia axis. Therefore, 2D PIV measurements

were conducted in plane with the cilium's deformation to examine the influence of motion asymmetry on the flow field created by cilia (see **Movies S1-S2**). The same experimental setup is used as during the ink dye tests, with the only difference that water is used as the cilium's actuation fluid, to avoid air bubble forming as discussed above. During each PIV test, 1024 images were taken at a frequency of 25 Hz and frames at the end of each actuation cycle are used to track the net displacement of the particles during that cycle. By cross-correlating these images, a time-averaged velocity field over a cycle is obtained and, to further decrease noise, these flow velocity fields are also averaged over the total number (5-10) of actuation cycles. To avoid transient effects, the measurements were taken while the cilium was already beating, so that the resulting average field is considered to be constant over time in order to plot the streamlines for visualizing the fluid flow. The difference between the flow fields for symmetric and asymmetric cilium beating patterns are plotted in **Figure 4a-4b** respectively (only the short segment is actuated in **Figure 4a**, and a 90° phase difference is used in **Figure 4b**), together with pictures of cilium's deformations and relative swept areas. As already qualitatively observed with dye tracing tests, the symmetrically beating cilium produces insignificant fluid motions. In comparison, the average velocities induced by the asymmetrical beating motion clearly creates a net fluid flow. The streamlines become more defined, following the direction of the effective stroke. The overall net flow velocities are computed in different points along the length of the channel by averaging the horizontal components of the velocity field over a vertical line perpendicular to the channel width. These net flow velocities are not constant along the flow direction, since our setup only allows to measure flow in a 2D plane. However, when far enough from the cilium, a uniform flow is observed, indicated by a constant net flow velocity. The flow speeds in this part of the channel are reported in **Figure 4c** for a reciprocal and nonreciprocal motion. For the symmetric test, flows speeds are in the order 10^{-4} mm min^{-1}, whereas in the asymmetric test a steady flow of two orders of magnitude higher is observed (0.04 mm min^{-1}).

In a subsequent test with the same asymmetric configuration, we decreased the pressure amplitude while maintaining the same frequency, which reduced the swept area from 10 to 4 mm². **Figure S3** shows the net fluid flow along the channel and a reduction of the flow by a factor 4 as a result of the reduced swept area. Therefore, it can be concluded that spatial asymmetry is vital for low-Reynolds fluid flow, and that orientational asymmetry alone only has a negligible effect, confirming experimentally the previous numerical works in the field [6] for cilia beating in-plane.

Further, the influence of the actuation frequency on flow propulsion for asymmetric beats is tested. For constant pressure amplitudes and phase lag, we compared the results for a variation of the beat frequency between 125, 250 and 500 mHz. In this experiment, the Reynolds number is not constant but it increases with frequency, to a maximum of 0.09 at 500 mHz, which is still within the Stokes flow regime. **Figure S4** displays the three flow fields obtained from these tests and all the values of the net fluid flow computed along the channel. These results are summarized in **Figure 5**, where panel (a) shows a drastic reduction of both swept area and orientation angle (average inclination of cilia during one stroke) with increased frequency. Both swept area and orientation angles are a measure of spatial and orientational asymmetry, and the graph shows a linear relation between these parameters and the frequency. There are two explanations for this trend based on dynamics effects. Firstly, viscous forces acting on cilia increase with higher actuation speeds, as also have been reported for magnetic beating cilia [34,52–54]. This effect is described by a dimensionless parameter called Sperm number [52,54,55], defined as the ratio between the viscous forces and the elasticity of the cilium. This parameter scales with the fourth root of the frequency (calculations in SI). Secondly, the elastic inflatable actuators have a limited bandwidth and therefore a reduced stroke above a specific actuation frequency [28]. As already deduced, orientational asymmetry alone does not play a significant role at these Reynolds numbers, thus the fluid flow is dominated by spatial asymmetry. Indeed, these tests show that there is

an optimum in fluid flow when varying actuation frequency and, as a consequence, swept area: the highest flow speeds appear at a actuation frequency of 250 mHz, where the cilium exhibits a spatial asymmetry that is optimal for efficiently propelling fluid. And although the swept area is larger at 125 mHz, this does not result in a larger net flow speed due to the lower frequency. On the contrary, at 500 mHz, the drastic reduction of the swept area decreases flow velocity.

In order to predict the optimal actuation frequency, we analyzed the single contribution of each parameter to the fluid flow and extracted a linear trend between two dimensionless parameters: the flow efficiency and the Reynolds number as shown in **Figure 5b**. Khaderi introduced the efficiency as the ratio between net area flow and swept area [6] and showed that it increases exponentially with the Reynolds number. In our experiment the Reynolds number is varying in a short range (0.02 – 0.09), justifying the linear interpolation. The net area flow is the net amount of fluid propelled and it is obtained by integrating the instantaneous fluid flux over the cycle time. For a fixed Reynolds this parameter is linearly proportional to the swept area, causing the efficiency to be independent of the swept area.

Since both swept area and efficiency can be expressed as function of the actuation frequency, and the net flow speed follows a cubic function of frequency (more details on the calculations in SI). This function is plotted in **Figure 5c** (red dashed-line), fitting our experimental data points on the cubic function. In **Figure 5d** we display a dimensionless version of our results that can be used for comparison with other artificial and biological ciliary propulsion systems, where net area flow is plotted against the Sperm number. As expected from the microswimmers theory [56], this analysis shows that there is an optimal Sperm number (Sp ≈ 5) that maximizes net flow. As shown in the figure inset, below this optimal frequency, an increase in spatial asymmetry is counteracted by fewer strokes. Above this optimal frequency, a reduction in spatial asymmetry reduces the overall net flow.

In this study, the cilia are still relatively large (16 mm in length), and there is an interest in scaling them down to match the size of cilia in biologic systems for future applications. There are examples in literature of elastic inflatable microactuators manufactured using soft lithography processes and SU8 molding that can be adapted to our design [39]. Further, we anticipate that a new design with a reduced inflated volume of the inner cavity of the actuators will also address the limited operation frequency of our current cilia. Nevertheless, the set-up presented in this paper has unique advantages in terms of fundamental understanding of the phenomena characterizing the ciliary propulsion. Thanks to the dimensionless parameters we can use the analysis at this scale to underpin the hydrodynamic interactions between cilia and viscous flow at any scale.

5. Conclusions

This paper describes an artificial cilium which mimics the spatial asymmetry observed in the in-plane beating motion of biological cilia. The cilium comprises two inflatable actuators, which provide two independent degrees of freedom to control the trajectory of the cilium's tip. This allows to implement different types of motion asymmetries and to study their effects on fluid flow. Our artificial cilia, are tested in a close-loop D-shaped channel, filled with glycerol to simulate the low-Reynolds conditions that characterize the fluid-cilia interaction of microorganisms. Both dye tracing tests and PIV measurements show that the asymmetric beating of the artificial cilium enhances the net fluid flow compared to reciprocal motion. Further, it has been shown that orientational asymmetry alone, has a negligible contribution to fluid flow and that the contribution of nonreciprocal motion is paramount to generate fluid propulsion. Moreover, we observed the existence of an optimal balance between actuation frequency and net flow speed. This corresponds to the optimum between net area flow and Sperm number that is generally observed in all artificial and biological ciliary system, when

the viscous hydrodynamic interactions overcome the cilium elasticity. In this work, thanks to the independent control over each parameter, we were able to extrapolate a cubic relation between net flow speed and frequency valid in the range of our experimental set-up. These experiments corroborate existing computational fluid dynamic models of cilia that have a planar motion and provide new insights in hydrodynamic interactions at different frequencies.

6. Experimental Section

Soft microactuators manufacturing: The 2DoF artificial pneumatic cilium used in this paper is fabricated through a silicon rubber casting process, where the entire actuator is made without the need of an additional bonding step to seal the inflatable void, as shown on **Figure S5**. A two-part mould is made out of aluminum using micromilling, which defines the external dimensions of the microactuator and the eccentricities of the inner chambers. Two tungsten carbide microrods with the dimensions of the inner chambers are placed in the bottom half of the micromold to complete it. A layer of liquid release agent (Devcon) is applied on both halves of the molds before pouring in uncured PDMS (Sylgard 184 – ratio 1:10). After closing the mold, PDMS is cured at 90 °C for 15 minutes. Demolding of the actuator is done with the use of ethanol as lubricant. The last step in the production process consists of connecting each internal chamber with a dedicated supply tube, by inserting two small tubes with the outer diameter 0.76 mm into the first 2 mm of the chamber, and gluing them into place with uncured PDMS.

Single cilium test setup: A single asymmetric pneumatic artificial cilium is connected to two software-controlled electro-pneumatic regulators (ITV0050-3MN-Q), one for each inflatable void. The pressure regulator imposes a trapezoidal pressure profile (linear ramp to a fixed value, followed by a linear decrease), where amplitudes, time period and phase difference can be set. This artificial cilium is positioned in a closed-loop fluid channel (**Figure S2**). The

channel is designed in a D-shape, where the cilium is placed in the straight section, having a width of 6 mm to assure 2D flow. One side wall of this section, colored gray on **Figure S2**, consists of a glass plate through which camera images can be taken for flow measurements. The two opposing straight sides, that are perpendicular to the imaging plane are also closed with glass plates to allow an external light source to illuminate the fluid. The rest of the channel loop is made out of black anodized aluminum to prevent unwanted light reflections. The artificial cilium protrudes from the top plate, with a dedicated oblong hole, that forms a liquid tight seal with the actuator itself. As such, the channel is completely watertight, and has water-solid interfaces on all sides. The channel itself is filled with glycerol, which has a viscosity of 10^3 times that of water. Thus, it is possible to decrease actuation times by the same factor and still have Re<1, so an effective stroke time that exceeds 160 s in water will only take 0.16 s in glycerol, as is deduced in SI.

Dye tracing: Ink lines are injected in the fluid and a light source placed to the side of the closed-loop channel lights up the fluid while a camera records the motion. The artificial cilium is actuated in two modes: symmetrically, where only the short segment is actuated, and asymmetrically where both segments are actuated having 90° phase difference in order to maximize the swept area.

PIV test: Fluorescent tracer polyethylene microspheres (45-53 μm UVPMS-BR from Cospheric) are dispersed evenly in the glycerol liquid, using surfactants. The images are acquired with a high-speed CMOS camera (HighSpeedStar 5 – LaVision) placed in front of the straight part of the channel, while the particles are illuminated with planar laser light (Dual Cavity Nd:YLF Pegasus-PIV laser from NewWave). In accordance with the dye tracing test, PIV measurements are conducted for symmetric and asymmetric actuation. During the multiple beating cycles of the cilium, images are acquired at a frequency of 25 Hz. The images are imported, analyzed and post-processed with the Matlab tool PIVlab [57].

Acknowledgements

References

[1] C. Brennen, Howert Winet, *Annu. Rev. Fluid Mech.* **1977**, *9*, 339.
[2] S. L. Tamm, *J. Cell Biol.* **1972**, *55*, 250.
[3] M. A. Sleigh, *Comp. Biochem. Physiol. -- Part A Physiol.* **1989**, *94*, 359.
[4] B. A. Afzelius, *J. Biophys. Biochem. Cytol.* **1961**, *9*, 383.
[5] E. M. Purcell, *Am. J. Phys.* **1977**, *45*, 3.
[6] S. N. Khaderi, M. G. H. M. Baltussen, P. D. Anderson, J. M. J. Den Toonder, P. R. Onck, *Phys. Rev. E - Stat. Nonlinear, Soft Matter Phys.* **2010**, *82*.
[7] S. N. Khaderi, M. G. H. M. Baltussen, P. D. Anderson, D. Ioan, J. M. J. Den Toonder, P. R. Onck, *Phys. Rev. E - Stat. Nonlinear, Soft Matter Phys.* **2009**, *79*.
[8] J. M. J. den Toonder, P. R. Onck, *Trends Biotechnol.* **2013**, *31*, 85.
[9] H. Ceylan, J. Giltinan, K. Kozielski, M. Sitti, Mobile microrobots for bioengineering applications. *Lab Chip* **2017**, *17*, 1705–1724.
[10] S. Kim, S. Lee, J. Lee, B. J. Nelson, L. Zhang, H. Choi, *Sci. Rep.* **2016**, *6*, 30713.
[11] P. Ribeiro, M. A. Khan, A. Alfadhel, F. Franco, S. Cardoso, A. Bernardino, A. Schmitz, *IEEE Robot. Autom. Lett.* **2017**, *2*, 971.
[12] Y. Wang, J. den Toonder, R. Cardinaels, P. Anderson, *Lab Chip* **2016**, *16*, 2277.
[13] A. Rockenbach, U. Schnakenberg, *J. Micromechanics Microengineering* **2017**, *27*, 015007.
[14] C. Y. Chen, L. Y. Cheng, C. C. Hsu, K. Mani, *Biomicrofluidics* **2015**, *9*, 1.
[15] J. den Toonder, F. Bos, D. Broer, L. Filippini, M. Gillies, J. de Goede, T. Mol, M. Reijme, W. Talen, H. Wilderbeek, V. Khatavkar, P. Anderson, *Lab Chip* **2008**, *8*, 533.
[16] N. Banka, Y. L. Ng, S. Devasia, *J. Med. Device.* **2017**, *11*, 031003.
[17] Y.-A. Wu, B. Panigrahi, Y.-H. Lu, C.-Y. Chen, *Micromachines* **2017**, *8*, 260.
[18] C. Y. Chen, C. C. Hsu, K. Mani, B. Panigrahi, *Chem. Eng. Process. Process Intensif.* **2016**, *99*, 33.
[19] B. A. Evans, A. R. Shields, R. L. Carroll, S. Washburn, M. R. Falvo, R. Superfine, C. Hill, C. Hill, N. Carolina, W. Virginia, V. Uni, W. Virginia, C. Hill, C. Hill, N. Carolina, *Nano Lett.* **2007**, *7*, 1428.
[20] M. Vilfan, A. Potocnik, B. Kavcic, N. Osterman, I. Poberaj, A. Vilfan, D. Babic, *Proc. Natl. Acad. Sci. U. S. A.* **2010**, *107*, 1844.
[21] J. Hussong, N. Schorr, J. Belardi, O. Prucker, J. Rühe, J. Westerweel, *Lab Chip* **2011**, *11*, 2017.
[22] C.-Y. Chen, C.-Y. Chen, C.-Y. Lin, Y.-T. Hu, *Lab Chip* **2013**, *13*, 2834.
[23] R. Marume, F. Tsumori, K. Kudo, T. Osada, K. Shinagawa, In *Japanese Journal of Applied Physics*; 2017; Vol. 56.
[24] C. Brücker, A. Keissner, *Exp. Fluids* **2010**, *49*, 57.
[25] K. Oh, J.-H. Chung, S. Devasia, J. J. Riley, *Lab Chip* **2009**, *9*, 1561.
[26] A. Keißner, C. Brücker, *Soft Matter* **2012**, *8*, 5342.
[27] A. Rockenbach, V. Mikulich, C. Br, U. Schnakenberg, C. Brücker, U. Schnakenberg, *J. Micromechanics Microengineering* **2015**, *25*, 125009.
[28] B. Gorissen, M. de Volder, D. Reynaerts, *Lab Chip* **2015**, *15*, 4348.
[29] J. Gray, *Proc. R. Soc. B Biol. Sci.* **1922**, *93*, 104.
[30] S. N. Khaderi, P. R. Onck, *J. Fluid Mech.* **2012**, *708*, 303.
[31] C. L. van Oosten, C. W. M. Bastiaansen, D. J. Broer, *Nat. Mater.* **2009**, *8*, 677.
[32] S. Sareh, J. Rossiter, A. Conn, K. Drescher, R. E. Goldstein, *J. R. Soc. Interface* **2012**,

10, 20120666.

[33] a R. Shields, B. L. Fiser, B. a Evans, M. R. Falvo, S. Washburn, R. Superfine, *Proc. Natl. Acad. Sci. U. S. A.* **2010**, *107*, 15670.

[34] Y. Wang, Y. Gao, H. Wyss, P. Anderson, J. den Toonder, *Lab Chip* **2013**, *13*, 3360.

[35] J. Belardi, N. Schorr, O. Prucker, J. Rühe, *Adv. Funct. Mater.* **2011**, *21*, 3314.

[36] S. Hanasoge, M. Ballard, P. J. Hesketh, A. Alexeev, *Lab Chip* **2017**, *17*.

[37] S. Hanasoge, P. J. Hesketh, A. Alexeev, *Soft Matter* **2018**, *14*, 3689.

[38] F. Connolly, C. J. Walsh, K. Bertoldi, *Proc. Natl. Acad. Sci.* **2016**, 201615140.

[39] B. Gorissen, C. Van Hoof, D. Reynaerts, M. De Volder, *Microsystems Nanoeng.* **2016**, *2*, 16045.

[40] S. Konishi, F. Kawai, P. Cusin, *Sensors Actuators, A Phys.* **2001**, *89*, 28.

[41] S. Konishi, S. Shimomura, S. Tajima, Y. Tabata, *Microsystems Nanoeng.* **2016**, *2*, 15048.

[42] A. J. M. Moers, M. F. L. De Volder, D. Reynaerts, *Biomed. Microdevices* **2012**.

[43] D. Han, H. Gu, J. wan Kim, S. Yokota, *Sensors Actuators, A Phys.* **2017**, *257*, 47.

[44] S. Wakimoto, K. Suzumori, K. Ogura, *Adv. Robot.* **2011**, *25*, 1311.

[45] A. Yamaguchi, K. Takemura, S. Yokota, K. Edamura, *Sensors Actuators A. Phys.* **2011**, *170*, 139.

[46] B. Gorissen, D. Reynaerts, S. Konishi, K. Yoshida, J.-W. Kim, M. De Volder, *Adv. Mater.* **2017**, 1604977.

[47] B. Gorissen, M. De Volder, A. De Greef, D. Reynaerts, *Sensors Actuators, A Phys.* **2011**, *168*, 58.

[48] B. Gorissen, W. Vincentie, F. Al-Bender, D. Reynaerts, M. De Volder, *J. Micromech. Microeng* **2013**, *23*, 45012.

[49] E. Milana, B. Gorissen, D. Volder, D. Reynaerts, *2018 IEEE Int. Conf. Soft Robot.* **2018**, 108.

[50] I. D. Johnston, D. K. McCluskey, C. K. L. Tan, M. C. Tracey, *J. Micromechanics Microengineering* **2014**, *24*, 035017.

[51] E. Lauga, T. R. Powers, *Reports Prog. Phys.* **2009**, *72*, 096601.

[52] S. Hanasoge, P. J. Hesketh, A. Alexeev, *Microsystems Nanoeng.* **2018**, *4*, 11.

[53] Y. Wang, Y. Gao, H. M. Wyss, P. D. Anderson, J. M. J. den Toonder, *Microfluid. Nanofluidics* **2014**, *18*, 167.

[54] C. P. Lowe, *Philos. Trans. R. Soc. Lond. B. Biol. Sci.* **2003**, *358*, 1543.

[55] C. Eloy, E. Lauga, *Phys. Rev. Lett.* **2012**, *109*.

[56] J. Elgeti, G. Gompper, *Proc. Natl. Acad. Sci. U. S. A.* **2013**, *110*, 4470.

[57] W. Thielicke, E. J. Stamhuis, *J. Open Res. Softw.* **2014**, *2*.
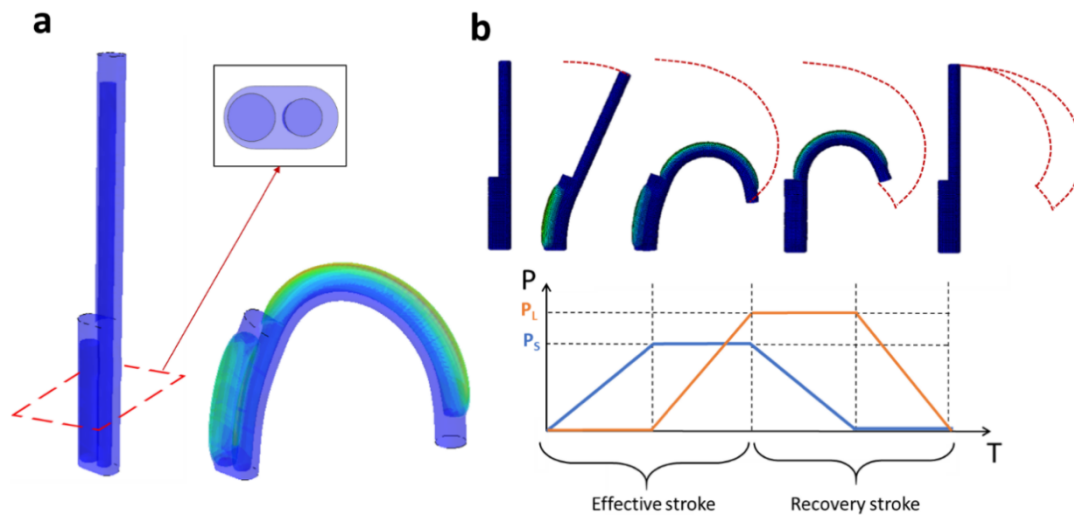
Figure 1. Design and operational principles of the artificial soft cilium (a). 3D view of cilium FEM simulations with cross-section view in the inset, showing the two inflatable chambers in the undeformed and deformed configuration. (b) Actuation scheme of a single cycle (effective and recovery stroke) of the artificial cilium (FEM simulations), with the two trapezoidal pressure waves with 90 ° phase difference which actuate in sequence the two elastic inflatable segments of the cilium. In dashed red line the swept area is represented.
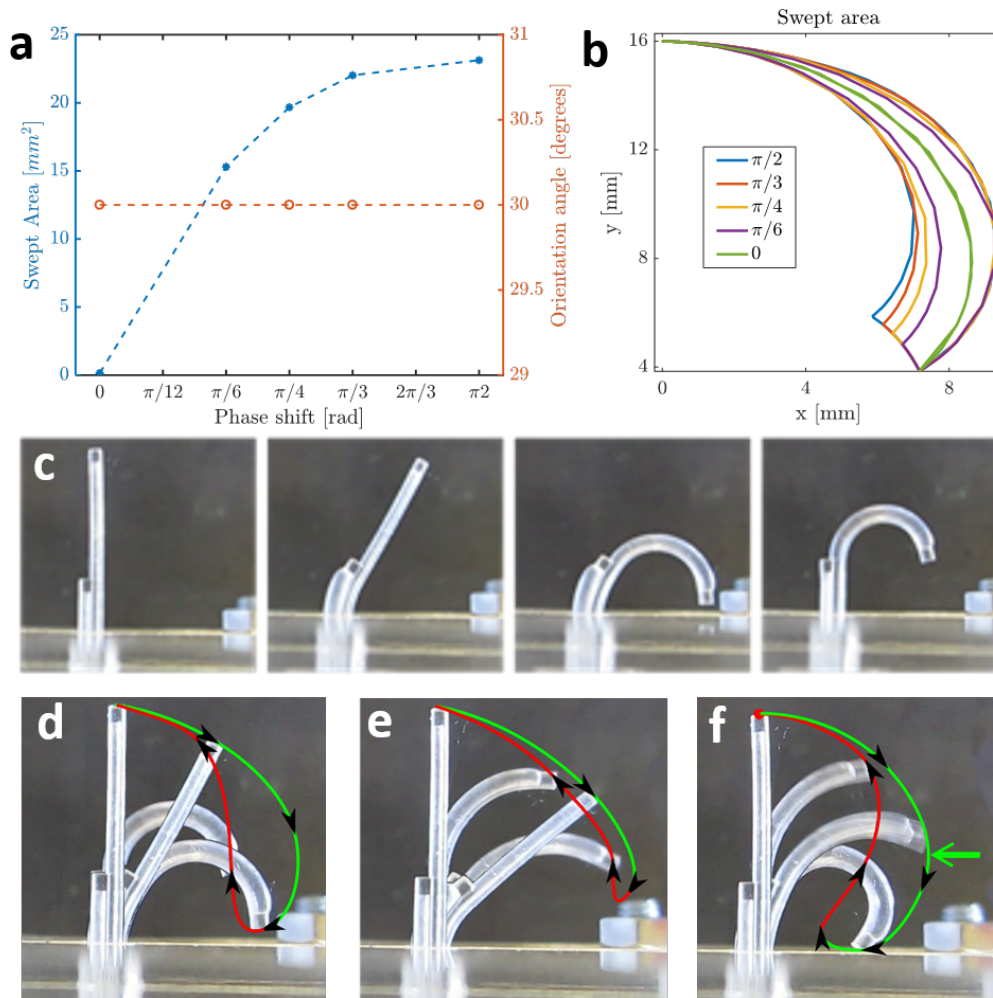
Figure 2. Simulation and experiment of cilia motion.(a) FEM analysis of the swept area. Swept area increases with phase difference between the two pressure waves for a maximum at 90° while orientational asymmetry does not vary. (b) Tip trajectories for the different phase differences. (c) cilium motion over one cycle. (d) the images are superimposed to obtain the tip trajectory of the effective (green) and recovery (red) strokes, enclosing a swept area. (e) Reduction of the swept areas due to lower inner pressures and (f) reduction of the swept area due an overloading of the actuator.
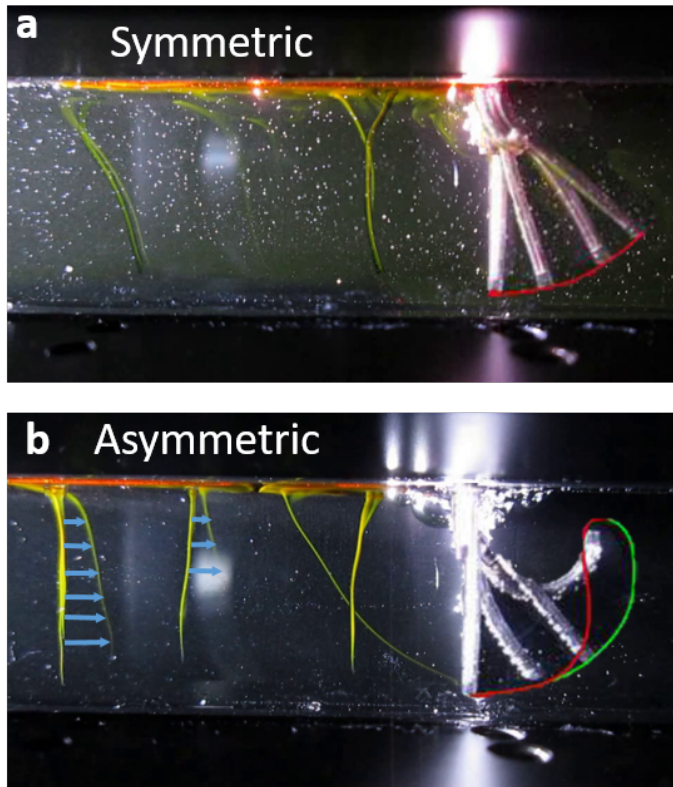
Figure 3. Images of the dye tracing test for symmetric (a) and asymmetric (b) motion, for a beating cilium at a frequency of 125 mHz. The final situations after 150 and 130 cycles are superimposed with the initial situation. For the symmetric case the ink lines did not move while in the asymmetric it is possible to observe a displacement of the ink.
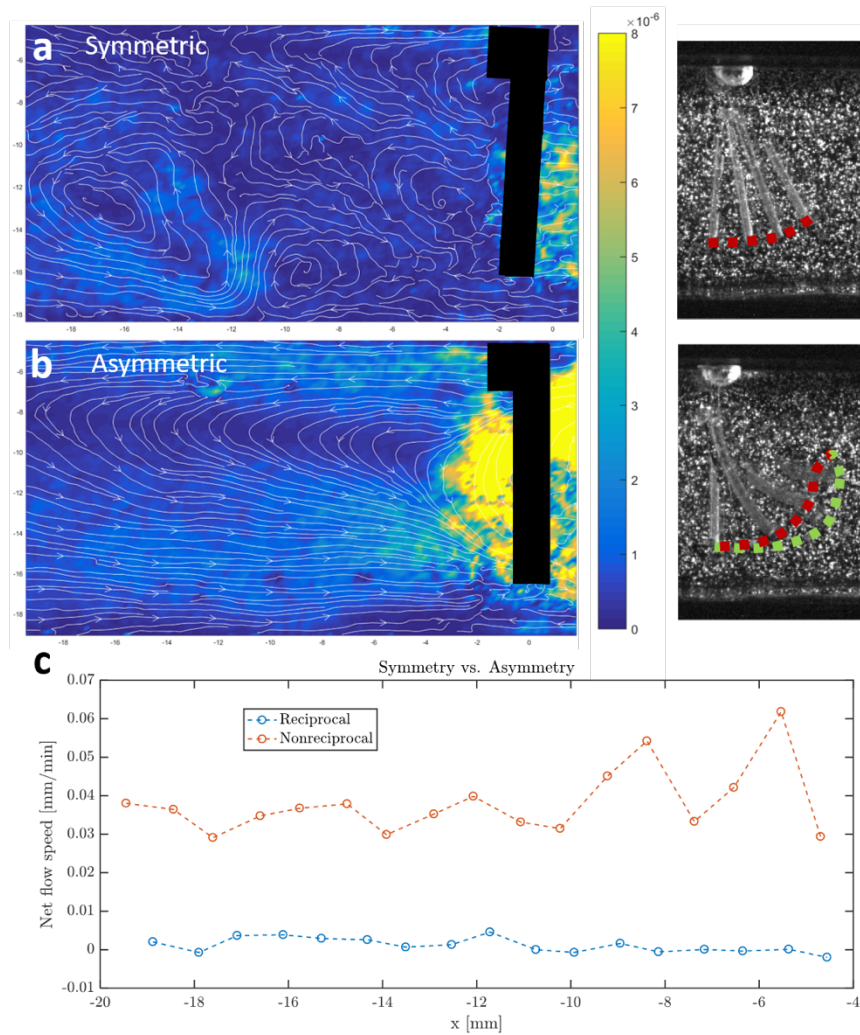
Figure 4. PIV measurement of the low Re velocity field averaged over a single cycle for symmetric (a) and asymmetric (b) cilium motion. The colorbar indicates the velocity magnitude in m/s. On the right there are superimposed images of the cilium motion tracing the tip trajectory for the two different configurations. (c) Net flow speed over different points of the channel for the reciprocal and nonreciprocal beating motion.
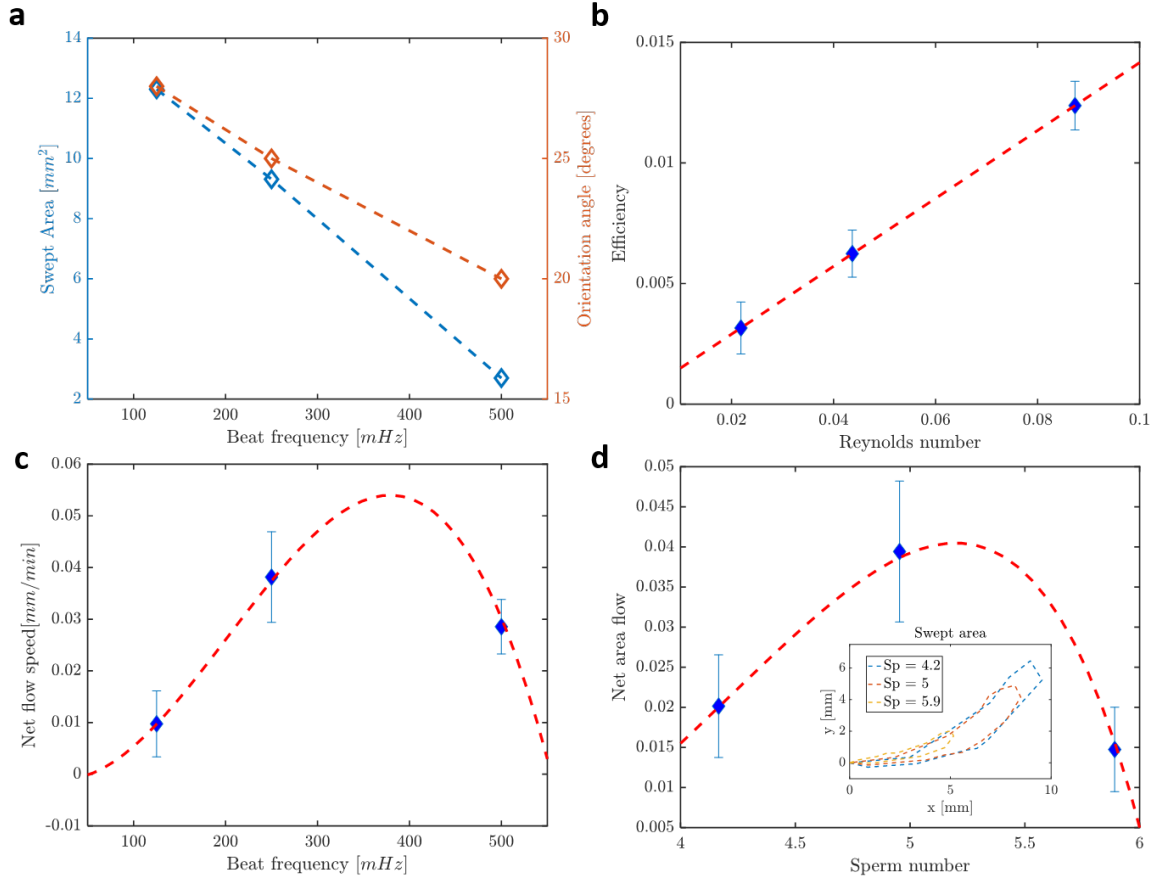
Figure 5. Comparison between three asymmetric configurations with different frequencies and same pressure amplitudes. (a) Swept area and orientation angle against frequency. (b) Linear trend between efficiency and Reynolds number (c) Averaged values of the net fluid flow in the channel. The red-dashed line corresponds to the cubic relation between net fluid speed and frequency. (d) Net area flow against Sperm number. The red-dashed line is a fitting based on the frequency dependencies of the parameters. In the inset tip trajectory enclosing the swept area for the three tests.